ELSEVIER

Journal of Hazardous Materials A79 (2000) 241–267

Journal of Hazardous Materials

www.elsevier.nl/locate/jhazmat

Explosion investigation of asphalt–salt mixtures in a reprocessing plant

Kazutoshi Hasegawa*, Yongfu Li[1]

National Research Institute of Fire and Disaster 14-1, Nakahara 3-Chome, Mitaka, Tokyo 181-8633, Japan

Received 1 July 1999; received in revised form 5 May 2000; accepted 7 June 2000

Abstract

Cause investigation of a fire and explosion at the nuclear fuel waste reprocessing plant indicated that self-heating ignition of an asphalt–salt-waste, bituminized, mixture (AS) caused the disaster. A 220 l drum was filled with the AS at a temperature of about 180°C. About 20 h later the drum ignited and burned as it was being cooled. It is estimated that the AS contained approximately 55 wt.% blown asphalt, 25 wt.% $NaNO_3$, 5 wt.% $NaNO_2$, 8 wt.% Na_2CO_3, 2 wt.% NaH_2PO_4, 1 wt.% Ba $(OH)_2$, 1 wt.% $K_4[Fe(CN)_6]$, and possibly 3 wt.% of other materials. To determine the reaction promoting factors and pertinent chemical reaction rates, self-reaction of the AS has been investigated by the use of a C80D heat flux reaction calorimeter. The oxidizing reactions with asphalt are ruled by $NaNO_2$ rather than by $NaNO_3$, in spite of a lower concentration of $NaNO_2$. The kinetic rates of the interfacial reaction between salt particles and asphalt for the reaction controlled and diffusion controlled steps have been formulated as a function of salt particle size for both $NaNO_2$ and $NaNO_3$. Numerical solution of the heat balance equations formulating the heterogeneous reaction scheme indicates that a runaway reaction occurs when the AS-filling temperature is 208°C for a drum filled with an AS mixture produced under standard operating conditions. Molecules containing intramolecular hydrogen, such as Na_2HPO_4 and $NaHCO_3$, do not oxidize asphalt directly, however, their presence chemically promotes the oxidizing reaction of $NaNO_2$. Moreover, $NaHCO_3$ decomposition which produces gases creates many micro holes in the interior of the salt particles. This in turn promotes the oxidizing reactions that are diffusion controlled. Finally, the consequence of a runaway reaction at 180°C or lower is qualitatively explained by taking into account the chemical effect of intramolecular hydrogen and the physical effect of the $NaHCO_3$ decomposition gases.

Keywords: Cause investigation; Self-heating ignition; Interfacial reaction; Bituminization; Radioactive wastes

* Corresponding author. Tel.: +81-422-44-8331; fax: +81-422-42-7719.
E-mail address: hasegawa@fri.go.jp (K. Hasegawa).
[1] Present address: Nanjing University of Science and Technology, Chemical College, Nanjing 210014, People's Republic of China.

0304-3894/00/$ – see front matter
PII: S0304-3894(00)00271-5

1. Introduction

On March 11, 1997, a fire and explosion accident occurred at the Bituminization Demonstration Facility (BDF) at the Tokai Works of the Power Reactor and Nuclear Fuel Development Corporation (PNC). The BDF stabilizes low-level radioactive liquid wastes generated at the Tokai Works Nuclear Fuel Reprocessing Plant. The BDF was totally damaged, including the radioactive material confinement function, and partially destroyed. As a result, radioactive materials contaminated the environment. The accident was the most severe in the history of Japanese nuclear power development — as a result, reliance on total safety in nuclear facilities suffered a severe setback. An exhaustive investigation into the cause of the accident was mandated. In response, immediately after the accident, an investigating committee was organized by the Nuclear Safety Bureau, Science & Technology Agency of Japan and chaired by Dr. A. Kanagawa who is an honorary professor at Nagoya University. One of the authors was a member of the committee. In the committee's report [1], the investigation of damage and the indirect cause of the accident were described in detail, but the direct cause of the outbreak of the fire was not clarified — this was pigeonholed as a problem to be solved in a long-term plan.

The purpose of this paper is to explain the direct cause of the accident, especially to clarify the chemical reaction mechanism that leads to the self-ignition of these asphalt–salt-waste mixtures in drums.

Present and past radioactive waste bituminizing processes exist or have existed in Belgium, Germany, France, Sweden, Switzerland, UK, USSR and Japan. They are divided into three types: batch, continuous extruder, and continuous thin-layer distillation. Most of them have experienced related accidents, including Harwell, UK (1967), Karlsruhe, Germany (1974), Saclay and Barseback, France (1977), Mol, Belgium (1981) [2], Tokai, Japan (1984), Saclay (1992), and Tokai (1997).

2. Accident summary

2.1. Bituminization Demonstration Facility and process

Low-level radioactive liquid wastes generated at the Reprocessing Plant are sent to the BDF [1]. In this facility, the aqueous radioactive wastes are incorporated into asphalt and dehydrated in an extruder in a batch treatment. The bituminized and stabilized product is poured into 220 l steel drums and stored. A flow diagram of the BDF process is shown in Fig. 1.

The BDF usually receives many types of low level wastes, but in a campaign (97M46-1) the receiving vessel (V21) had received only evaporator-condensates wastes (MA wastes) from the No. 1 low-level radioactive waste evaporating vessel, and phosphoric acid wastes (ST wastes) from the waste solvent treatment facility. The MA wastes had been stored in the V21 vessel and at the time of the accident a small amount of the ST wastes was added to the vessel in the middle of the campaign. The goal of the campaign was to increase the efficiency of drum filling.

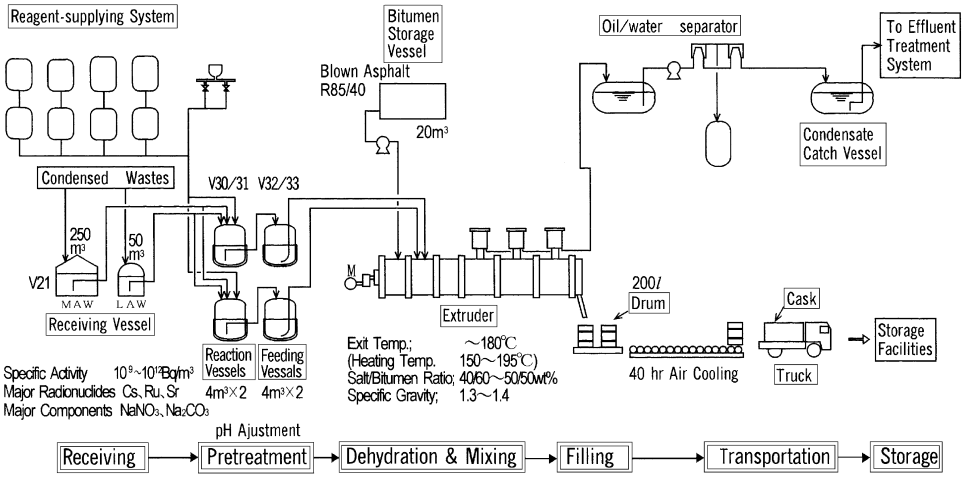

Fig. 1. Flow diagram of the Bituminization Demonstration Facility process.

In the BDF process, the wastes stored in vessel V21 are transferred to one of two reaction vessels (V30/V31, 50°C) where chemical reagents are added to precipitate cesium (Cs), strontium (Sr), and iodine (I) radionuclides and to adjust the pH to a prescribed value 9.0. The treated wastes are then fed to the extruder via one of two feeding vessels (V32/V33, 50°C). The two routes through these two vessels are used alternately. Approximately 4 m^3 of waste is treated in each batch.

Dehydration of the waste and mixing of the dehydrated product with asphalt are carried out by an extruder with eight zones. In zones 3–6, water is evaporated from the mixture at approximately 170–187°C. Three domes (condensers) installed in zones 4–6 remove evaporated water. Zone 8 is a discharge pipe through which the mixed product of asphalt and solid salt waste is poured into a 220 l drum at about 180°C. Drum filling takes place on a turntable in a filling room (R152, floor area: 26.6 m × 4.7 m, ceiling height: 4.25 m). Usually 10–12 drums are filled in each batch. The extruder, equipped with four 120 mm-diameter, 5262 mm-long screw shafts, was manufactured by Werner & Pfleiderer Co. in Germany and was put into operation in April 1982.

The filled drums are naturally cooled at an ambient temperature of about 50°C in the filling room, and then, after capping, are transported to the storage facilities by cask.

2.2. Summary of accident

2.2.1. Operating conditions

Prior to the accident, the extruder had been operated at a standard waste feed rate of 200 l/h [1]. However, in campaign 97M46-1 the waste feed rate was decreased to 160 l/h. The asphalt feed rate was correspondingly decreased to maintain the ratio of asphalt to salts at about 55%.

2.2.2. 11 March accident events

At 10.06 h, on 11 March 1997, an outbreak of fire was observed in the BDF filling room (R152). According to the testimony of an observer, a pillar of fire approximately 2 m high shot up from a drum that was being cooled in the room, and soon after pillars of fire were observed on several drums. Approximately 5 min later, the observer opened a water sprinkling system valve for about 1 min. At about 10.13 h, the observer thought that the fire was extinguished.

From the onset of the fire until several minutes later, the air-blowers in the ventilation system for the cells and radiation shielded areas shut down, since the fire plugged the filters upstream of the blowers. Subsequently the cell ventilation system shut down. Consequently, the entire ventilation system for the BDF shut down.

At 20.04 h, about 10 h after the outbreak of fire, an explosion occurred unexpectedly in the BDF. The explosion damaged many of the BDF's windows and doors. Broken windows and other openings caused by the explosion released clouds of smoke. The fire continued in the R152 room as evidenced by the smoke being released. Radioactive materials were also released to the surroundings with the smoke. Visible smoke emissions from the fire ceased at 23.20 h.

2.2.3. Damage

The damage, which spread in all directions within the BDF building (four stories with two basements, building area: about 14.5 m × 54 m), radiated from the R152 room, in which a partition wall, a removable roof, and very thick steel doors were blown down. In the most remarkably damaged room (A235), which was directly above the R152 room, a reinforced concrete wall buckled outward and its reinforcing rods were exposed by the blast. Equipment, windows, doors, etc. were damaged and destroyed everywhere in the building. The ventilation systems were also found to be damaged everywhere — ducts were bent down, their connections were broken, and the filters were heavily damaged.

A survey was conducted on 129 people who might have been exposed to radioactive materials in the domain of the PNC Tokai Works. A very small quantity of radioactive ^{134}Cs and ^{137}Cs, at a maximum of approximately 0.004 and 0.02 mSv, respectively, was detected in the bodies of 37 persons. The total amount of radioactive ^{137}Cs discharged to the surroundings was estimated to be 1–4 GBq based on data from monitoring of the surroundings.

3. Reactivity of $NaNO_3$ and $NaNO_2$ with asphalt

To evaluate the minimum temperature of the runaway reaction (MTRR) for a 220 l drum filled with bituminized waste product (at the MTRR) and then cooled at an ambient temperature of 50°C, the kinetics of the oxidation–reduction reaction for the bituminized wastes product must first be determined. In particular, the individual oxidation reaction rates of asphalt with sodium nitrate and sodium nitrite were determined for various particle sizes of the dehydrated salt waste. The behavior of the runaway reaction in a drum was then modeled and numerically simulated to determine the MTRR.

3.1. Experiment and results

3.1.1. Experiment

To obtain more information on the mechanism of oxidation than would be obtainable using only adiabatic conditions, thermal analysis was performed under a variety of conditions. Furthermore, a high thermal analysis instrument sensitivity was required so that the thermal output due to heat generation could be measured at as low temperature range as possible [3]. For this purpose, a heat flux reaction calorimeter (C80D) with high detection sensitivity manufactured by SETARAM in France was used in order to maintain a very small and constant positive temperature gradient (rate of temperature increase) or a precise constant temperature. The C80D has the following general specifications: a temperature range of ambient to 300°C, a heat flux detection limit of 10 μW, an approximate time constant of 250 s for a full experimental vessel and an instant energy detection limit of 1 mJ. The volume of the experimental vessel was 8.5 ml and the vessel was pressure-proofed to 100 bar. A reference vessel was filled with alumina whose mass was identical to the sample mass.

Analysis of the composition of the real aqueous wastes indicated they were mostly the same as the simulated-mixed aqueous wastes shown in Table 1. However, the real wastes

Table 1
Simulated-bituminized wastes samples

Symbol	Unit	SBW-1[a]	SBW-2	SBW-3	SBW-4	SBW-5	SBW-6
Simulated-mixed aqueous wastes[b]							
$NaNO_3$	g/l	250 (26.42)	250 (26.42)	250 (26.42)	250 (26.42)	250 (26.42)	250 (26.42)
$NaNO_2$	g/l	50 (5.28)	50 (5.28)	50 (5.28)	50 (5.28)	50 (5.28)	50 (5.28)
Na_2CO_3	g/l	80	80	80	80	80	80
NaH_2PO_4	g/l	20	20	100	20	20	20
Precipitation step							
$Ba(OH)_2{\cdot}8H_2O$	g/l	10.3	18.93	18.93	18.93	18.93	18.93
pH adjustment with 13N nitric acid		pH≒9	None	None	pH=9	None	pH=9
$K_4Fe(CN)_6{\cdot}3H_2O$	g/l	9.72	9.72	9.72	9.72	9.72	9.72
$NiSO_4{\cdot}6H_2O$	g/l	12.09	12.09	12.09	12.09	12.09	12.09
Na_2SO_3	g/l	0	0	0	0	0	3.80
$AgNO_3$	g/l	0	0	0	0	0	0.0556
Drying temperature[c]	°C	–	About 100	About 100	About 65	About 65	About 65
Salt particle size	μm	–	≤53	≤53	≤20	≤20	≤20
Bituminization step							
Total salt content	wt.%	45.00	45.00	53.44	45.00	45.00	45.00
Method of preparation		[d]	[e]	[e]	[e]	[e]	[e]

[a] Produced by PNC in November 1996.

[b] Numbers in parentheses indicate wt.% in bituminized sample.

[c] Temperature at which the aqueous salt solution was dried to recrystallization.

[d] Produced by slowly adding treated aqueous wastes to asphalt (see Table 3) of 170–180°C with stirring, i.e. dehydration and mixing, then by cooling naturally.

[e] Produced by mixing homogeneously ground salt with asphalt (see Table 3) at about 100°C in a flask and cooling naturally.

additionally contained approximately 1.7 g/l Na_3PO_4, 16.8 g/l NaOH, 200 ppm tributyl phosphate (TBP), and 800 ppm dibutyl phosphate (DBP), as well as the radioactive materials. The chemicals contained in the real waste and the conditions for the precipitation treatment were nearly the same as for sample SBW-6. But, the real bituminized step of very fast dehydration was not actualized in each simulated samples. The compositions and preparation conditions for samples are given in Tables 1–3. More than 90% of the counted salt particles in the real bituminized products were smaller than 25 μm in size. Accordingly, the salt particle sizes in the samples SBW-1 (salt particles visible to the naked eye), SA-NAB, and SA-NIB seem not to match those in the real bituminized waste product.

3.1.2. Results

The heat release onset temperatures for sample SBW-1 were measured by PNC to be 370 and 336°C using a SC-DSC (sealed cell-differential scanning calorimeter) and an ARC (Accelerating Rate Calorimeter), respectively [1]. However, according to the results of the C80D experiment, the heat release begins gradually at about 200°C and continues to completion at 295°C under the experimental condition of a constant temperature increase rate of 0.01°C/min. The heat release responses are shown in Fig. 2. The total heat release is calculated to be 1282.6 J/g from the area between the base line and the heat release curve.

In order to examine the independent reactivities of sodium nitrate and sodium nitrite with asphalt, C80D calorimeter tests for samples SA-NAA, SA-NAB, SA-NIA and SA-NIB (see Table 2) were carried out at a constant temperature increase rate of 0.01°C/min. as shown in Fig. 3. The heat release onset temperature for sodium nitrite looks considerably lower than that for sodium nitrate. After the sample temperature reaches the onset temperature, the sample containing the smaller size salt particles immediately exhibits remarkable heat release. In contrast, the sample with larger salt particle sizes generates heat gradually and relatively slowly. Namely, the salt particle size appears to have a noticeable effect on reactivity.

The total heats of reaction of sodium nitrate and sodium nitrite with asphalt are 369.876 kJ/mol $NaNO_3$ and 156.009 kJ/mol $NaNO_2$, respectively.

3.2. Reaction models and reaction rates

3.2.1. Pseudo zero-order reaction

Since the asphalt and salts in the bituminized product are not mutually soluble, the reaction between them will occur at the interface. The rate-determining step for this reaction must then be chemical reaction controlled in the initial stages, followed by a diffusion-controlled process. Moreover, the dehydrated waste salts are composed of various types of salts that may be not only oxidants, but also catalysts and catalyst poisons. Therefore the reaction mechanism seems too complicated to be formulated. However, the simplifying assumption that the reaction obeys a pseudo zero-order reaction is commonly used for analyzing thermal ignition behavior in the initial stages when the consumption of reactants can be counted as negligible. Using this assumption, the overall heat flow is then expressed by

$$\frac{\mathrm{d}H}{\mathrm{d}t} = M_0 \Delta H_\mathrm{R} A_\mathrm{p} \exp\left(\frac{-E_\mathrm{p}}{RT}\right). \tag{1}$$

Table 2
Salt–asphalt mixture samples

Symbol	Unit	SA-NAA	SA-NAB	SA-NIA	SA-NIB	SA-NI0	SA-NI1	SA-CH0	SA-CH1	SA-PH0	SA-PH1	SA-PH2
Salt												
$NaNO_3$	wt.%	26.42	26.42	–	–	–	–	–	–	–	–	–
$NaNO_2$	wt.%	–	–	5.28	5.28	5.28	5.28	5.28	5.28	5.28	5.28	5.28
Na_2CO_3	wt.%	–	–	–	–	–	–	5.28	–	–	–	–
$NaHCO_3$	wt.%	–	–	–	–	–	–	–	5.28	–	–	–
$Na_3PO_4{\cdot}12H_2O$	wt.%	–	–	–	–	–	–	–	–	5.28	–	–
Na_2HPO_4	wt.%	–	–	–	–	–	–	–	–	–	5.28	–
NaH_2PO_4	wt.%	–	–	–	–	–	–	–	–	–	–	5.28
Drying temperature[a]	°C	–	–	–	–	–	90	60	60	60	60	50
Salt particle size (wt.%)												
>430 μm		–	8.35	–	7.11	–	–	–	–	–	–	–
430∼320 μm		–	35.28	–	59.47	–	–	–	–	–	–	–
320∼290 μm		–	41.62	–	26.57	–	–	–	–	–	–	–
290∼232 μm		–	13.64	–	6.00	–	–	–	–	–	–	–
232∼153 μm		–	1.11	–	0.85	–	–	–	–	–	–	–
≤53 μm		100	–	100	–	–	–	–	–	–	–	–
≤20 μm		–	–	–	100	100	100	100	100	100	100	100
Asphalt[b]	wt.%	73.58	73.58	94.72	94.72	94.72	94.72	89.44	89.44	89.44	89.44	89.44
Bituminization method			[c]	[c]	[c]	[c]	[c]	[c]	[c]	[c]	[c]	[c]

[a] Temperature at which an aqueous solution of salt was dried to re-crystallization, –; use of a solid chemical reagent.
[b] See Table 3.
[c] Mixture was produced by mixing homogeneously ground salt with asphalt at about 100°C in flask and cooling naturally.

Table 3
Asphalt[a]

Production			
Name	Blown asphalt (Trade name: AD Compound R85/40)		
Maker	Showa Shell Sekiyu K.K.		
Composition (wt.%)		Physical characteristics	
Saturated compounds	22.8	Softening point	82°C
Aromatics	34.8	Penetration (25°C)	36 mm/10
Resins	15.8	Flash point (coc)	316°C
Asphalten	26.8	Soluble in ethane trichloride	99.47 wt.%
		Ductility (25°C)	4 cm
		Specific gravity (25/25°C)	1.018

[a] After taking off light ingredients from crude oil, oxidative polymerization is done by blowing air into a distillation still, i.e. blown asphalt is air-oxidized straight asphalt.

By applying a pseudo zero-order reaction to the heat flux data obtained for sample SBW-1 in the temperature range 196–208°C, the relationship between the normalized heat-release rate and the inverse temperature is plotted with a high correlation as shown in Fig. 4. From the regression line, the activation energy and the frequency factor are estimated to be $E_p=1.779\times10^5$ J/mol and $A_p=1.079\times10^{13}$ l/s, respectively. Consequently, the thermokinetic equation for the plot in Fig. 4 is the basic formula required for determination of the MTRR.

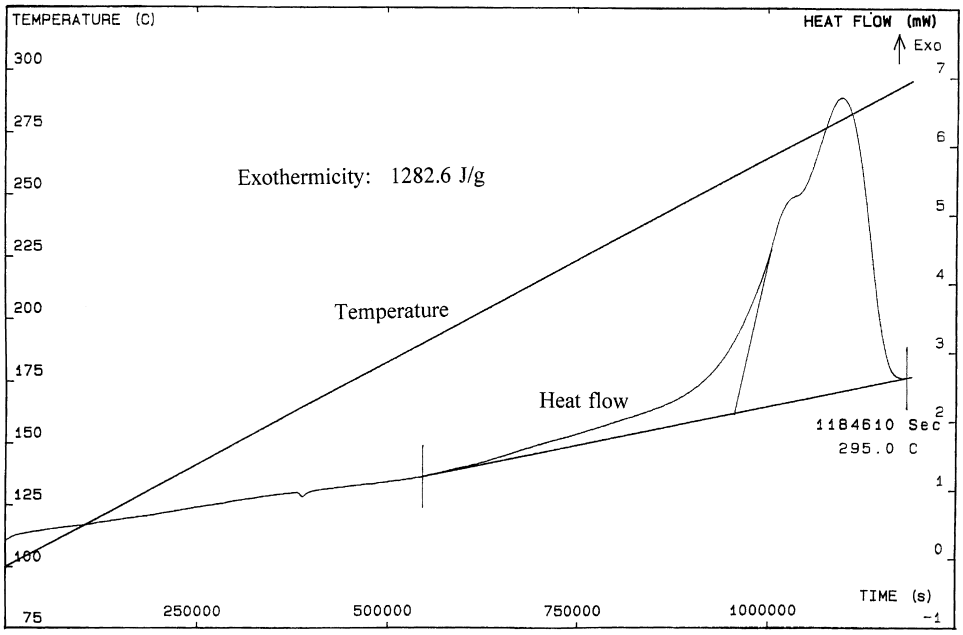

Fig. 2. Heat flow versus time at a constant temperature increase rate of 0.01°C/min (sample SBW-1, 0.5000 g in nitrogen).

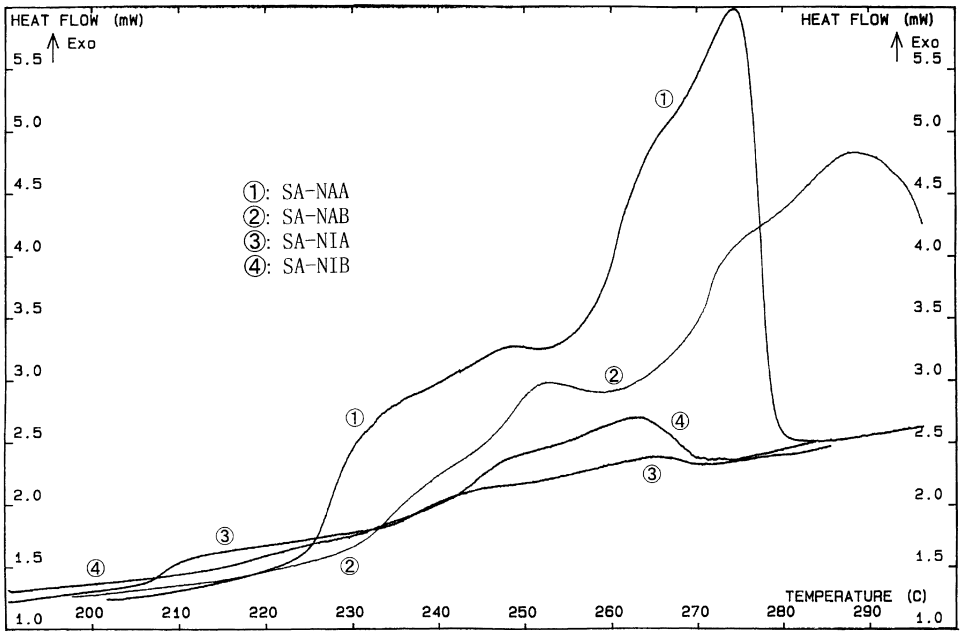

Fig. 3. Heat flow versus temperature at a constant temperature increase rate of 0.01°C/min (0.5000 g sample in nitrogen).

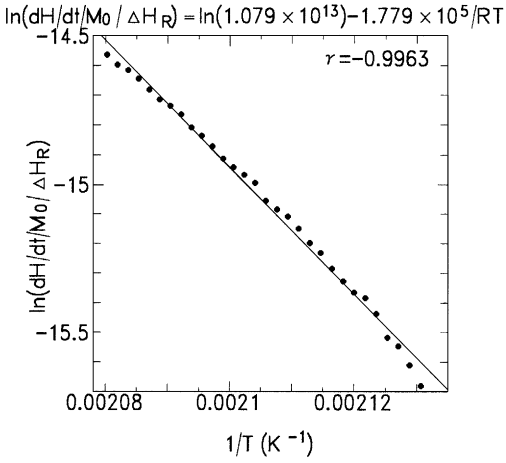

Fig. 4. Arrhenius plot to determine the kinetic parameters of the pseudo zero-order reaction (sample SBW-1).

3.2.2. Interfacial reaction on a salt particle in asphalt

3.2.2.1. Chemical reaction-controlled rate. For a salt particle contained in asphalt, the rate-determining step is chemical-reaction-rate-controlled in the initial stages of the reaction when, for a very short time, the asphalt is in direct contact with the oxidizing salt. During this stage, the mass conversion ratio, x, is nearly equal to zero, i.e. $x=0$, and the concentration of oxidizing salt at the asphalt–salt interface is maintained at approximately the same concentration as in the surroundings at a distance from the interface, i.e. $[S]_{\text{surface}}=[S]_0$. Therefore, according to a first-order reaction expression, the heat flow is expressed by

$$\frac{\mathrm{d}H}{\mathrm{d}t} = -\frac{\mathrm{d}[S]_{\text{surface}}}{\mathrm{d}t} V_{\text{surface}} M_0 \Delta H_{\text{R}} = M_0 \Delta H_{\text{R}} \text{ Area } [S]_0 A d_{\text{surface}} \exp\left(\frac{-E}{RT}\right), \quad (2)$$

where 'Area' is calculated from the salt particle size, based on an assumed spherical model.

3.2.2.2. Diffusion process-controlled rate. After the initial stage, a product layer, i.e. a diffusion layer, may exist between the asphalt and the oxidizing salt. The diffusion rate of a salt molecule must be faster than that of an asphalt molecule, since the salt molecular size is smaller than that of asphalt. Therefore, according to a one way diffusion model for the salt molecule (i.e. the reaction interface exists on the asphalt side) the diffusion process is formulated for this later stage as the rate-determining step. By the use of Fick's law, the overall heat flow is approximately expressed by the following equation:

$$\frac{\mathrm{d}H}{\mathrm{d}t} \fallingdotseq \Delta H_{\text{R}} \text{ Area } M_0 [S]_0 D_0 \exp\frac{(-E_{\text{D}}/RT)}{\delta}. \quad (3)$$

The thickness of the diffusion layer, δ, is related to product volume and also to the conversion ratio of salt, x, as

$$\delta = r_{\text{asphalt}} - r_{\text{salt}} = r_{\text{salt},0}\left(1 + \text{O}_{\text{balance}} \frac{\rho_{\text{salt}}}{\rho_{\text{asphalt}}} x\right)^{1/3} - r_{\text{salt},0}(1-x)^{1/3}, \quad (4)$$

where $r_{\text{salt},0}$ is the initial radius of a spherical salt particle, r_{salt} and r_{asphalt} are the inner and outer radii of the spherical shell of product, respectively, ρ_{asphalt} is the asphalt density (1.025 ± 0.025 g/ml), and ρ_{salt} is the salt density ($NaNO_3$, 2.260 g/ml, and $NaNO_2$, 2.168 g/ml). Assuming that the molecular formula of asphalt is C_nH_{2n}, the oxygen balances (O_{balance}) are calculated to be 0.1372 for $NaNO_3$ and 0.1014 for $NaNO_2$.

3.2.2.3. Overall heat flow for the whole reaction. The overall heat flow through the whole reaction can be calculated from the sum of Eqs. (2) and (3). Therefore, the rate of depletion of the salt concentration at the reaction interface is expressed by

$$\begin{aligned}\frac{\mathrm{d}[S]_{\text{surface}}}{\mathrm{d}t} &= D_0 \exp\left(-\frac{E_{\text{D}}}{RT}\right)\left(\frac{([S]_0 - [S]_{\text{surface}})/\delta}{d_{\text{surface}}}\right) - A \exp\left(-\frac{E}{RT}\right)[S]_{\text{surface}} \\ &= k_{\text{D}}\left(\frac{([S]_0 - [S]_{\text{surface}})/\delta}{d_{\text{surface}}}\right) - k_{\text{R}}[S]_{\text{surface}}. \end{aligned} \quad (5)$$

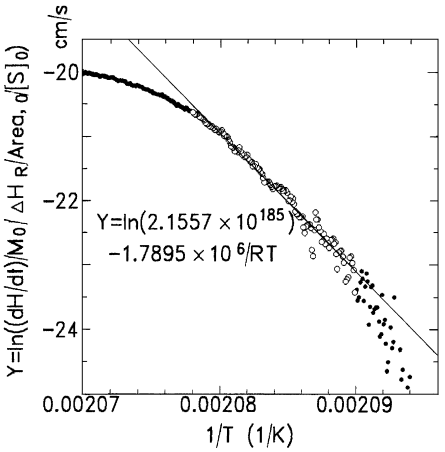

Fig. 5. Arrhenius plot to determine the kinetic parameters of the rate-determining chemical reaction for the oxidation–reduction reaction between sodium nitrite and asphalt (sample SA-NIA).

The solution of Eq. (5) is

$$[S]_{\text{surface}} = \frac{k_D/\delta[S]_0 + k_R d_{\text{surface}}[S]_0 \exp[-(k_D/\delta/d_{\text{surface}} + k_R)t]}{(k_D/\delta + k_R d_{\text{surface}})}. \quad (6)$$

By substituting $[S]_{\text{surface}}$ into $[S]_0$ of Eq. (2), the equation for the overall heat flow through the whole reaction is obtained

$$\frac{d[H]}{dt} = M_0 \Delta H_R \text{ Area } [S]_{\text{surface}} A d_{\text{surface}} \exp\left(-\frac{E}{RT}\right). \quad (7)$$

By applying the experimentally obtained individual heat flows (as shown in Fig. 3) in the initial stage, and in the later stage to Eqs. (2) and (3), respectively, the kinetic parameters E and Ad_{surface} for the chemical reaction, and the kinetic parameters E_D and D_0 for the diffusion process can be determined by calculating the slope and the intercept from the regression line for the plotted data. Typical examples are shown in Figs. 5 and 6, respectively. A list of the kinetic parameters obtained for samples SA-NAA and SA-NIA are given in Table 4.

Once the reaction mechanism and its kinetic parameters are determined, we can simulate the experimental results of heat flow for all stages, from the rate-determining initial chemical reaction to the rate-determining diffusion process, by numerically solving simultaneously Eqs. (6) and (7). However, as d_{surface} was the only unknown parameter, it was varied as a parameter in the simulation calculations. As a result, when $d_{\text{surface}} \leq 1.0$ μm, all simulated results were closely coincident with the experimental results. Therefore, d_{surface} was considered to be approximately 1.0 μm.

It seems odd that the values of the activation energy shown in Table 4 appear to be too large. Other values of the kinetic parameters do not always look reasonable as well. However, even if the mechanisms and the corresponding values of the kinetic parameters are not correct, as long as the conditions (especially the temperature range) for which the obtained rate equations would be applicable are almost equal to the experimental conditions, it would be reasonable to use them in the model. For instance to predict the MTRR for a

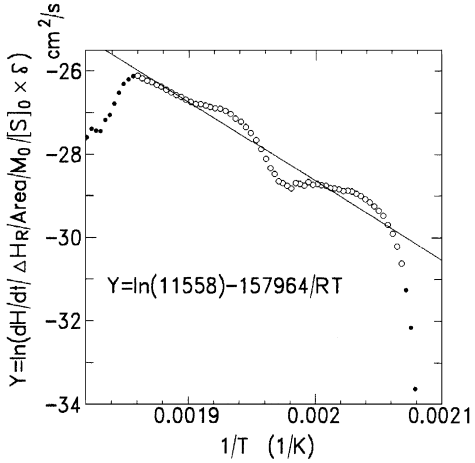

Fig. 6. Arrhenius plot to determine the kinetic parameters of the rate-determining diffusion process for the oxidation–reduction reaction between sodium nitrite and asphalt (sample SA-NIA).

filled drum. The simulated results agreed well with the C80D experimental results obtained for several conditions that varied the constant rate of temperature increase and the constant temperatures. Therefore the simulation could be expected to closely approximate the actual phenomenon.

3.3. Simulation of product-filled drum

3.3.1. Heat balance equation

The heat balance equation for a drum filled with bituminized waste product is composed of three heat flow terms as given in the following expression:

$$\sum \left(\frac{\mathrm{d}H}{\mathrm{d}t}\right)_{\mathrm{EX}} + \sum \left(\frac{\mathrm{d}H}{\mathrm{d}t}\right)_{\mathrm{HE}} + \left(\frac{\mathrm{d}H}{\mathrm{d}t}\right)_{\mathrm{HC}} = 0, \tag{8}$$

Table 4
Kinetic parameters of interfacial reactions

Sample		SA-NAA[a]	SA-NIA[a]
Chemical reaction			
E	kJ/mol	933.673	1.7895×10^{3}
Ad_{surface}	1/s	1.6814×10^{88}	2.1557×10^{185}
Temperatures	°C	216–229	205–208
γ		−0.9974	−0.9902
Diffusion process			
E_{D}	kJ/mol	218.753	11.558
D_0	cm^2/s	5.3523×10^{9}	1.5796×10^{5}
Temperatures	°C	234–275	210–264
γ		−0.9935	−0.9746

[a] Assuming $r_{\mathrm{salt},0}=26.5\,\mu\mathrm{m}$.

where the first term expresses the exothermicity of chemical reactions, the second heat transfer, and the third self-heating. The exothermicity obeys Eq. (1) or Eq. (7) according to the reaction model. The heat transfer is composed of heat exchanges within the reacting material itself, between the reacting material and the drum vessel, and between the drum vessel and its surroundings. Accordingly, it is described by a generalized and simplified equation

$$\left(\frac{\mathrm{d}H}{\mathrm{d}t}\right)_{\mathrm{HE}} = -\kappa S_{\mathrm{a}} \frac{\mathrm{d}T}{\mathrm{d}r_{\mathrm{d}}}, \tag{9}$$

where κ is the thermal conductivity of the reacting material or steel drum material depending on the location for which the calculation is being done. The coefficient for heat transfer between the drum vessel and surroundings is obtained from the Nusselt number, *Nu*. *Nu* is estimated from the model for heat transfer across a vertical surface by natural convection. The endothermicity resulting from heat absorption by the reacting material depends on its heat capacity as follows:

$$\left(\frac{\mathrm{d}H}{\mathrm{d}t}\right)_{\mathrm{HC}} = -C_p M_0 \frac{\mathrm{d}T}{\mathrm{d}t}, \tag{10}$$

where the specific heat, C_p, can be determined from the C80D experimental results obtained for a constant rate of temperature increase, i.e. the base line for the heat flow versus temperature curve.

3.3.2. Simulation of runaway reaction

If it is assumed that the AS drum is cylindrical and the thermal conductivity of the media is very low, a one-dimensional cylindrical coordinate system can also be assumed. With these assumptions, Eq. (7) is rewritten as

$$\frac{\partial^2 T}{\partial r_{\mathrm{d}}^2} + \frac{1}{r_{\mathrm{d}}}\frac{\partial T}{\partial r_{\mathrm{d}}} + \frac{\dot{q}}{\kappa} = \frac{1}{\alpha}\frac{\partial T}{\partial t}, \tag{11}$$

where $\dot{q}$ is the rate of heat generation per unit volume and $\alpha = \kappa/\rho/C_p$. Under the initial conditions of the presumed temperature, T_{i}, of the product-filled drum, an ambient temperature $T_0 = 50^{\circ}\mathrm{C}$, and the given boundary conditions, the Eq. (11) simultaneous equations are numerically and successively solved, using the physicochemical property constants shown in Table 5. These equations are solved as functions of the elapsed time, *t*, and radial distance, r_{d}. The minimum temperature, T_{i}, at which the calculated temperature, *T*, can run away steeply from an upward trending temperature is taken as the MTRR. Typical examples of simulation results are shown in Figs. 7 and 8. These examples illustrate how the temperature of bituminized product behaves as a function of time and drum radius. The conclusive results obtained by the simulations are summarized in Table 6.

3.3.3. Discussion of simulation results

In regard to the oxidation–reduction reaction of the salts and asphalt, both sodium nitrate and sodium nitrite were considered to play a principal role as oxidants in view of their composition. However, the simulation results prove that during the induction period of the

Table 5
Simulation conditions and physicochemical property constants

Sample	Sodium nitrate/asphalt	5.28/94.72
Ambient temperature	T_0 (°C)	50
Density	ρ (g/cm^3)	1.30
Specific heat	C_P (J/K/s)	$1.180+0.002092\times T$
Thermal conductivity of sample	κ (J/cm/K/s)	0.05
Thermal conductivity of drum(steel)	κ (J/cm/K/s)	$1.13-0.00109\times T$
Thermal conductivity of air	κ (J/cm/K/s)	3.83×10^{-4}
Heat of reaction	ΔH_R (J/mol $NaNO_2$)	156020
Salt particle size	$r_{salt,0}$ (μm)	20
Chemical reaction rate	$d[S]_{Surface}/dt = -M_0 \Delta H_R \text{ Area } [S]_0 Ad_{Surface} e^{-E/RT}$	
	$Ad_{Surface}$ (1/s)	2.1557×10^{185}
	E (J/mol)	1.7895×10^{6}
Rate of diffusion process	$d[S]_{Surface}/dt = D_0 e^{-E_0/RT}(([S]_0 - [S]_{Surface})/\delta)/d_{Surface}$	
	D_0 (1/s)	1.5796×10^{6}
	E_D (J/mol)	11558
Radius of drum	R_0 (cm)	28
Thickness of drum	(cm)	0.16
Nusselt number	$Nu_L = (hL/\kappa) = 0.795(Pr/(1+2Pr^{1/2} + 2Pr))^{1/4}((L^3\beta g(T_w - T_\infty)/\nu^2)Pr)^{1/4}$	
Height of drum	L (cm)	71.5
Prandtl number	Pr	0.70
Kinetic viscosity	ν (cm^2/s)	0.239
Mesh number on radial axis		60

runaway reaction sodium nitrite reacts with asphalt exclusively in spite of the fact that sodium nitrite is a much smaller proportion of the salt than sodium nitrate.

As indicated by the simulation results, the MTRR is limited by and clearly depends on the particle size of the oxidizing salt. A comparatively higher MTRR for sample SBW-1 would result from both the larger salt particle sizes for this sample and the difference in reaction mechanism. Since most of the salt particles in the real bituminized product were smaller than 25 μm in size, the MTRR of 228.8°C of sample SBW-1 would not be representative of the MTRR of real bituminized product. More realistically, the MTRR of real bituminized product must be close to 208°C. Therefore, when a drum is filled with the ordinary bituminized product having a temperature 180°C, it would be safe, although the safety margin at this temperature is not considered large enough. In the final analysis, the accident, i.e. the runaway reaction in the drum, could not have occurred if the bituminized product had been produced under normal operating conditions.

4. Oxidation-promoting effects

This section presents the results of the investigation of the oxidation-promoting effects and decreased MTRR resulting from changes in the standard operating conditions for the waste bituminizing process.

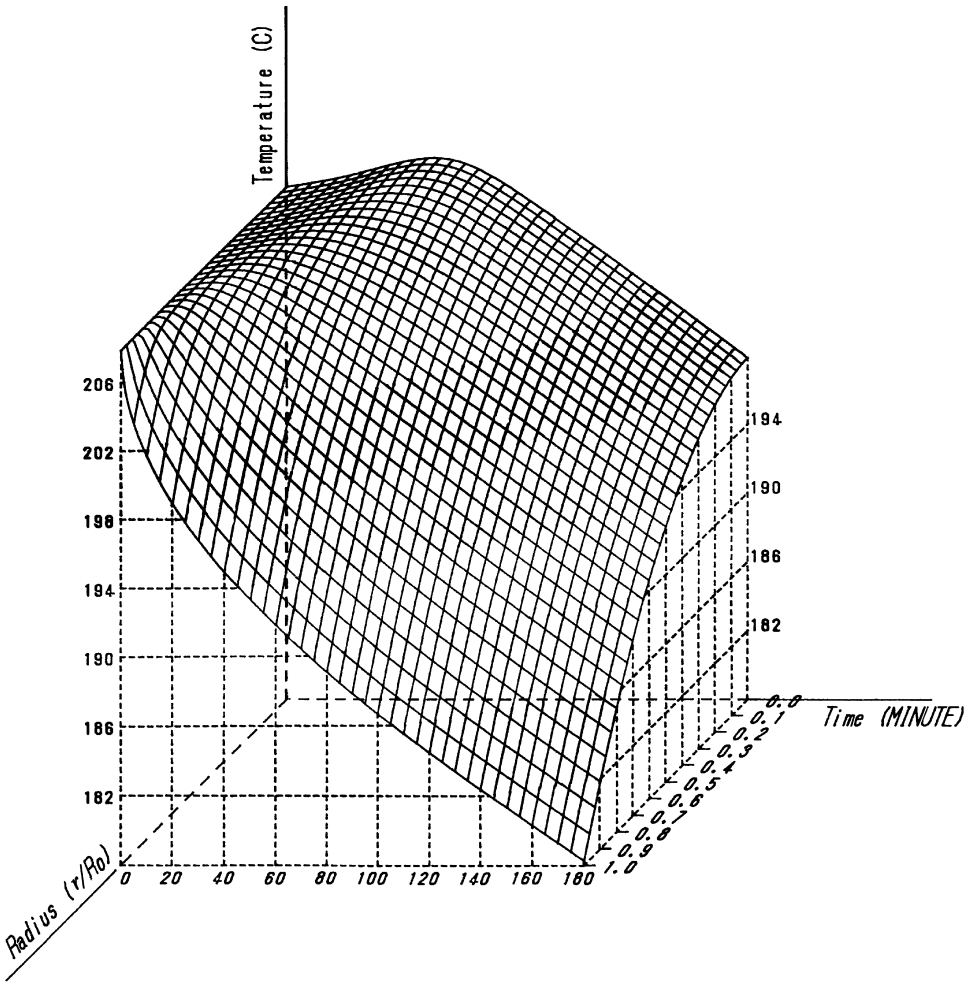

Fig. 7. Simulation of temperature changes on the time and drum radius axes for a drum filled with bituminized waste product (T_i=207.90°C, physicochemical property constants shown in Table 5).

4.1. Promoting effect of intramolecular hydrogen

4.1.1. Experimental results

Fig. 9 gives the C80D experimental results for samples SA-NI0, -NI1, -CH0, -CH1, -PH0, -PH1 and -PH2. The experimental conditions included a constant temperature increase rate of 0.05°C/min and a sample mass of 1000 g. The effects of individual non-oxidizing salts on the sodium nitrite oxidation of asphalt were examined.

4.1.2. Effect of intramolecular hydrogen on onset temperature

The onset temperatures of heat generation for the samples SA-NI0 and -NI1 were each about 210°C. The onset temperatures for samples SA-CH0 and -PH0, which did not con-

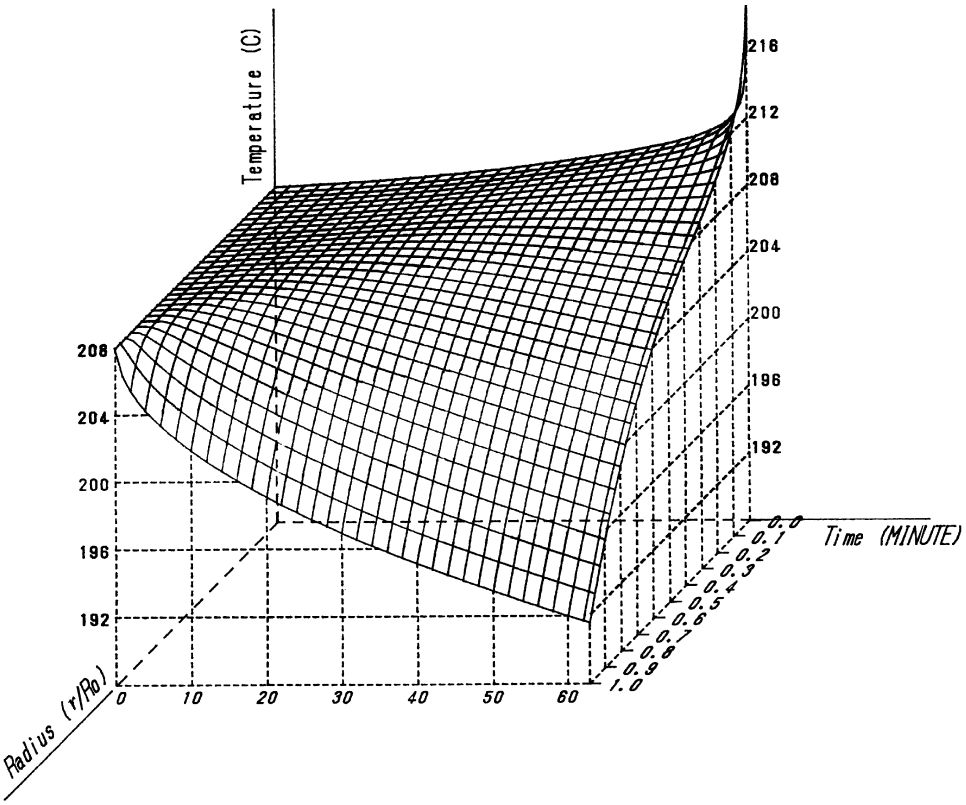

Fig. 8. Simulation of temperature changes on the time and drum radius axes for a drum filled with bituminized waste product (T_i=208.0°C, physicochemical property constants shown in Table 5).

tain intramolecular hydrogen in the salt ingredients, are almost equal to those of samples SA-NI0 and -NI1. On the other hand, the samples SA-CH1 and -PH1, containing salts having one intramolecular hydrogen, yield heat release onset temperatures of approximately 145°C, which is considerably lower than those for samples SA-NI0 and -NI1. Moreover, for the sample SA-PH2, containing a salt having two intramolecular hydrogens, the onset temperature is decreased remarkably to about 90°C.

In conclusion, it has been verified that sodium nitrite in salt mixtures has increased oxidizing power as the number of intramolecular hydrogens increases in the non-oxidizing salt molecules. There is a possibility that the intramolecular hydrogen contained in a non-oxidizing salt can locally produce nitrous acid at the asphalt–salt interface by chemical action on sodium nitrite. Nitrous acid, a stronger oxidizing agent than sodium nitrite, could lower the onset temperature.

4.2. Promoting effect of $NaHCO_3$

Sample SA-CH1 begins to generate heat not only at a relatively low temperature but also according to the distinctive heat flow curve illustrated in Fig. 9. This result is interpreted to

Table 6
Simulation of drum filled with bituminized product

	Simulated bituminized product	Sample of SBW-1	Sodium nitrate/asphalt[b] =26.42/73.58			Sodium nitrite/asphalt[b] =5.28/94.72			Sodium nitrate/sodium nitrite/ asphalt[b]=26.42/5.28/68.30		
Conditions	Salt particle size (μm)	–	20	53	1000	20	53	1000	20	53	1000
	Reaction model	Pseudo zero-order reaction	Interfacial reaction			Interfacial reaction			Interfacial reaction		
Results	MTRR[a] (°C)	228.8	225.2	227.5	235.2	208.0	209.1	212.3	208.0	209.1	212.3

[a] The minimum temperature of the poured product that will result in a run-away reaction when the drum is cooled at an ambient temperature of 50°C.
[b] See Table 3.

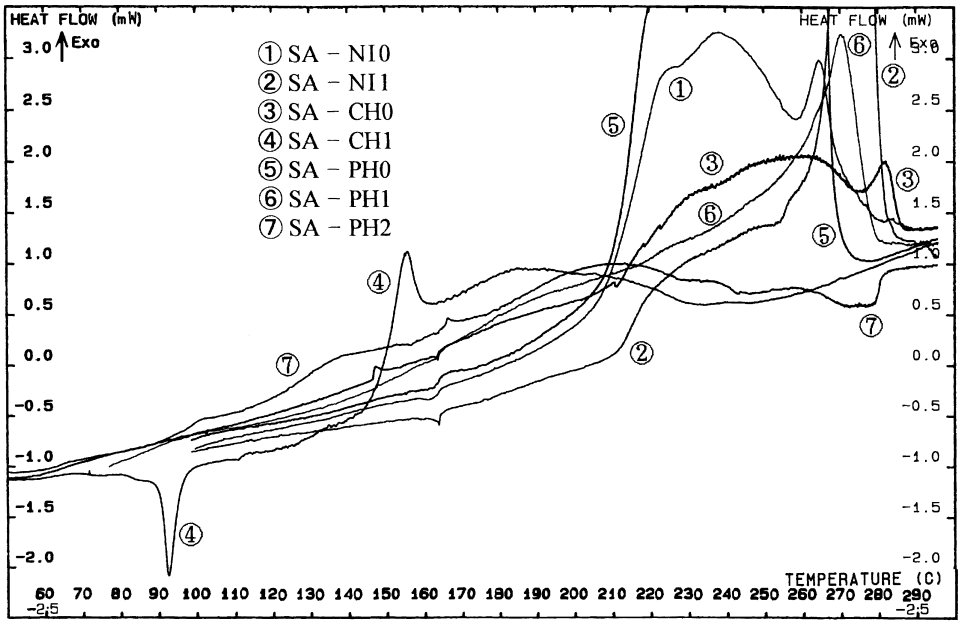

Fig. 9. Heat flow versus temperature at a constant temperature increase rate of 0.05°C/min (1.000 g sample in nitrogen).

mean that sodium hydrogencarbonate contributes much toward promoting both the chemical reaction and diffusion in the respective rate-determining stages of the interfacial reaction. On the other hand, just before 100°C, sample SA-CH1 exhibits an endothermic valley during which sodium hydrogencarbonate decomposes, generating carbon dioxide gas and water vapor. When these gases escape from a salt particle, many micro pores result and the salt particle becomes porous, i.e. a 'honeycomb' structure. The honeycomb structure would greatly accelerate the diffusion step of the interfacial reaction.

4.3. Behavior of simulated-bituminized samples

4.3.1. C80D Experimental results

The C80D experimental results for the simulated bituminized samples SBW-2, -3, -4, -5 and -6 listed in Table 1 are shown in Figs. 10 and 11. The compositions of these samples, especially SBW-6, simulate the real bituminized product as closely as possible.

The heat release of the SBW-2 sample begins gradually at a temperature of about 200°C and is completed at about 265°C, which is substantially different from the behavior of samples SA-NAA, which is a mixture of only sodium nitrate and asphalt, and SA-NIA, which is a mixture of only sodium nitrite and asphalt. The carbonate and/or phosphate in sample SBW-2 are thought to have some kind of oxidation promoting effect.

Sample SBW-3 contains sodium dihydrogenphosphate in a quantity five times more than the other samples. It was found that when the composition of phosphate increases, the onset

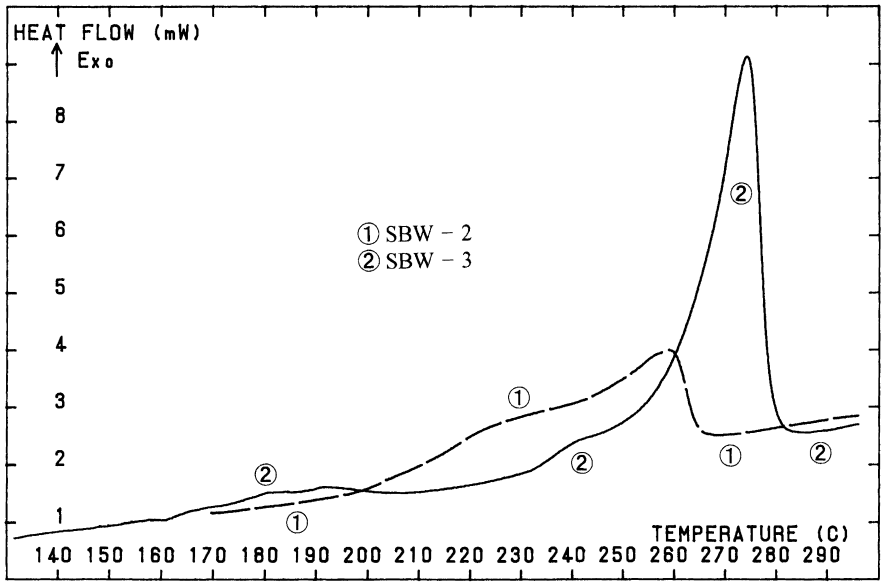

Fig. 10. Heat flow versus temperature at a constant temperature increase rate of 0.01°C/min (0.500 g sample in nitrogen).

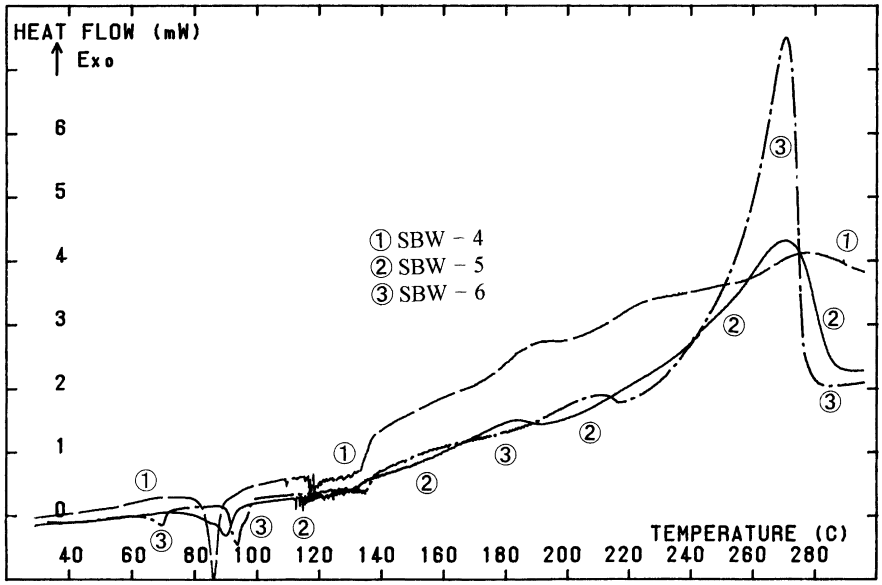

Fig. 11. Heat flow versus temperature at a constant temperature increase rate of 0.02°C/min (0.5000 g sample in nitrogen).

temperature of heat release decreases but the rate of heat release is slow in the initial stage and disappears occasionally.

Three samples, SBW-4, -5, and -6, each have an endothermic valley within the temperature range of 80–100°C (Fig. 11), resulting from the decomposition of sodium hydrogencarbonate. Sodium carbonate and sodium dihydrogenphosphate dissolved in water are known to form mostly sodium hydrogencarbonate and disodium hydrogenphosphate, respectively, according to the equilibrium diagram at a pH of nine [4]. In order to include sodium hydrogencarbonate as a solid salt, these simulated aqueous wastes were dried to recrystallization at considerably lower temperature than the decomposition temperature. For these three simulated bituminized waste samples, small rapid oscillations were observed in the heat release curves between about 120 and 140°C. This was thought to be caused by gases spurting from different locations on the asphalt surface. During the period of decomposition, the salt particle structure could also have changed into a honeycomb structure. Consequently, heat generation onset occurs suddenly at the quite low temperature of about 140°C and it presents a considerable heat flow. The differences in behavior between the three samples during the latter stage are thought to probably depend on subtle differences in the process of how the asphalt and salt particles are made.

In conclusion, there are hardly any differences in the composition of these simulated bituminized samples, but their oxidation–reduction reactivities are different and depend strongly on how the salt particles are made. Determining whether sodium hydrogencarbonate exists in the salt particles must be a major contributing factor in determining the heat release rate of the bituminized waste product.

4.3.2. Fine structure of salt particles

The geometrical structure of the salt particles in the bituminized product is significant for controlling the diffusion rate that in turn will affect the reactivity. The fine structure of the simulated sample SBW-4 was examined by an EPMA JXA-880ORE electron probe microanalyzer scanning electron microscope (SEM) manufactured by JEOL in Japan. The SEM results are shown in Figs. 12 and 13.

A variety of sizes and shapes of salt particles with planar surfaces can be seen in Fig. 12. The photo in Fig. 13 was taken after the sample had been kept at approximately 100°C for fourteen hours. The state of this treated sample was thought to correspond to that of the samples in Fig. 11 just before the onset temperature of the heat release curve. Many micro pores are observed in the particle structure, i.e. honeycomb-structured particles are observed. It is clear that the pore holes are created when gases generated by decomposition of sodium hydrogencarbonate disrupt the structure. The resulting particle volume is increased and the particle looks fragile.

4.4. Discussion of promoting effects

The real reaction mechanism of the simulated bituminized sample is too complicated to be formulated from the C80D results recorded in Fig. 11. Even if the reaction mechanism could be formulated, it is envisioned to be composed of immensely complicated equations having many unknown parameters. Accordingly, it would be impossible to solve the equations for the SBW-4, -5 and -6 samples. The onset temperatures for samples SBW-1, SA-NAA, and

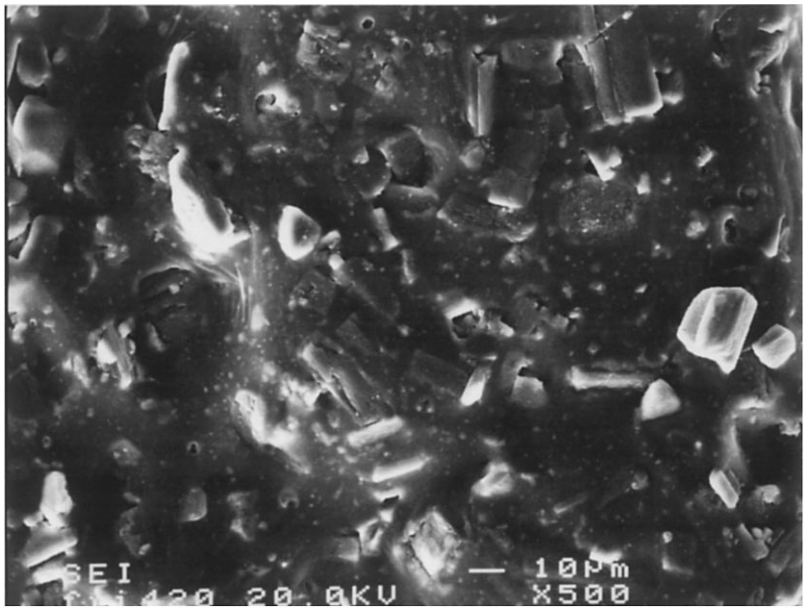

Fig. 12. SEM photo (sample SBW-4).

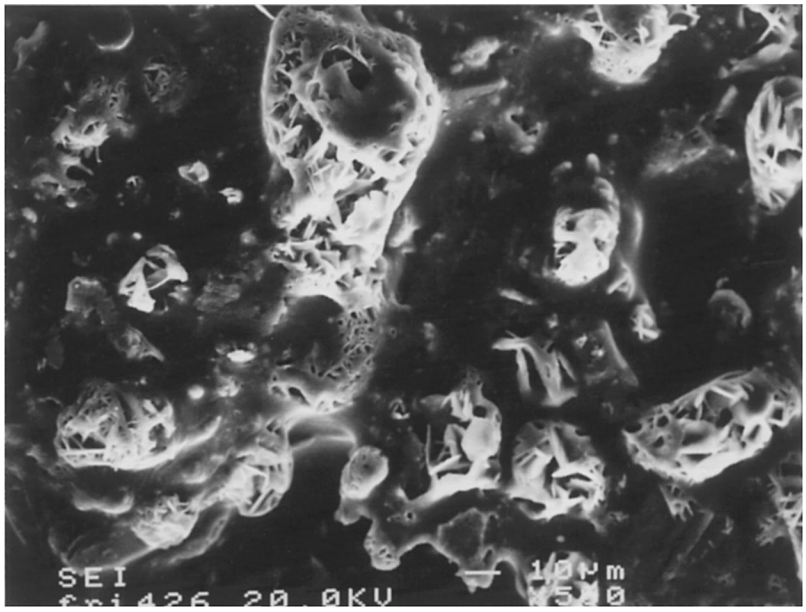

Fig. 13. SEM photo (sample SBW-4 heated for 14 h at 100°C).

-NIA are approximately 200, 225 and 208°C, respectively, and the corresponding MTRRs are 228.8, 227.5 and 209.1°C, respectively. On the basis of the relationship between the onset temperatures for heat release in the C80D results for these samples and MTRRs, the MTRRs for the SBW-4, -5 and -6 samples are similarly estimated to be a temperature of roughly 140°C. Of course, the initial slope of the heat flow curves should also be considered in this estimation.

If a drum is filled with product similar to the SBW-4, -5 and -6 samples at a normal controlled temperature of 180°C, it is evident that a run away reaction will occur easily in the drum and an outbreak of fire must be expected. However, the MTRR will decrease strongly according to the amount of sodium hydrogencarbonate retained in a solid particle when dehydration has ended in the extruder. When the aqueous wastes evaporate rapidly (i.e. the evaporation rate is faster than the decomposition rate of sodium hydrogencarbonate) sodium hydrogencarbonate must be left in the solid salt particle for a short time even if the temperature is high enough to decompose sodium hydrogencarbonate.

5. Irregularities in operation

There were three differences from the standard operation, i.e. three irregularities, in the twenty-ninth batch (B29) of campaign 97M46-1. Such irregularities had not been experienced since the plant started up in 1982.

5.1. First irregularity

The receiving vessel (V21) intermittently received 1 m^3 of phosphoric acid wastes (ST wastes) in addition to the usual MA wastes, which had been a change since March 3, 1997 from the campaign plan. In the next process step for reaction vessel V31, strontium (Sr) was coprecipitated with barium carbonate ($BaCO_3$) by first adding barium hydroxide ($Ba(OH)_2$). However, both barium carbonate and barium hydrogen phosphate ($BaHPO_4$) are insoluble in water (solubilities of 2.0×10^{-3} and $(1.0–2.0)\times10^{-2}$ g/100 ml (25°C), respectively). Therefore, when barium hydroxide was added to the wastes in which both carbonate and phosphate exist, the following reactions are thought to have competed with each other

$$NaHCO_3 + Ba(OH)^2 \rightarrow BaCO_3 \downarrow + NaOH + H_2O, \quad (12)$$

$$Na_2HPO_4 + Ba(OH)^2 \rightarrow BaHPO_4 \downarrow + 2NaOH. \quad (13)$$

By receiving phosphoric acid wastes (ST wastes), the concentration of phosphate became so high in the wastes that the barium salt precipitates could be higher in phosphate and lower in carbonate than in the ordinary operation. Indeed, the $PO_4{}^{3-}$ concentration of 7.7 g/l measured in the wastes before transfer to vessel V31 was much higher than the ordinary concentration range of 5 mg/l to 1.4 g/l. As a result, the dissolved carbonate in the wastes in the V31 reaction vessel is considered to have increased. This suggests that, after the pH=9 adjustment, the wastes sent to the extruder had a much higher concentration of sodium hydrogencarbonate than usual.

5.2. Second irregularity

An air sparger in the V21 receiving vessel was used to agitate the waste before sampling. A few minutes later, transfer of the wastes to the V31 reaction vessel was initiated. The transfer had usually started at one day after the agitation. Because of the length of time that elapsed after agitation, there is a possibility that the transferred wastes contained precipitates containing highly soluble sodium carbonates. These solid phase sodium carbonates could dissolve back into the wastes as the solution concentration of carbonate ion decreases as it is removed from solution by the precipitation step. As a result, immediately after treatment these wastes would contain a higher concentration of sodium carbonates than the ordinary wastes. Afterward, the sodium carbonate behavior is the same as described above.

5.3. Third irregularity

The extruder had usually been operated at a standard waste feed rate of 200 l/h. However, in campaign 97M46-1, the feed rate was changed to 160 l/h after the twenty-sixth batch (B26). Accordingly, the evaporation, i.e., dehydration, of the waste was completed earlier than under the normal conditions. Specifically, the salt was thought to have been recrystallized at an earlier stage in the process. Indeed, the recorded amount of condensed water removed by the third condenser was much less than the normal amount after the feed rate was decreased. This means that the time for sodium hydrogencarbonate decomposition in the liquid phase was shortened. Consequently, there is a possibility that sodium hydrogencarbonate was left partly in a crystalline form and then decomposed in the later stages of the extruder and/or in a drum. The extruder power source torque had been recorded as being at a higher level during processing of batch B29. This probably means that salt particles were produced in earlier stages of the extruder.

5.4. Discussion of irregularities

The three irregularities each cause sodium hydrogencarbonate to exist in the waste salt particles. These three irregularities are necessary conditions for sodium hydrogencarbonate to exist in the salt particles but not sufficient conditions for the accident. Even if the hydrogencarbonate existed in the particles, it is impossible to evaluate how the three irregularities contribute toward retention of the hydrogencarbonate in the particles. Moreover, how these three irregularities each contribute directly toward lowering the MTRR or which irregularity is the most important factor in lowering the MTRR could not be determined.

5.5. Witness reports

The following additional evidence pertinent to the accident was observed [1].

- As a drum was filled with the bituminized product, the product poured into the drum were characterized by an operator as looking ‘soft’ in comparison with the usual appearance.
- The product was steaming, which was unusual.

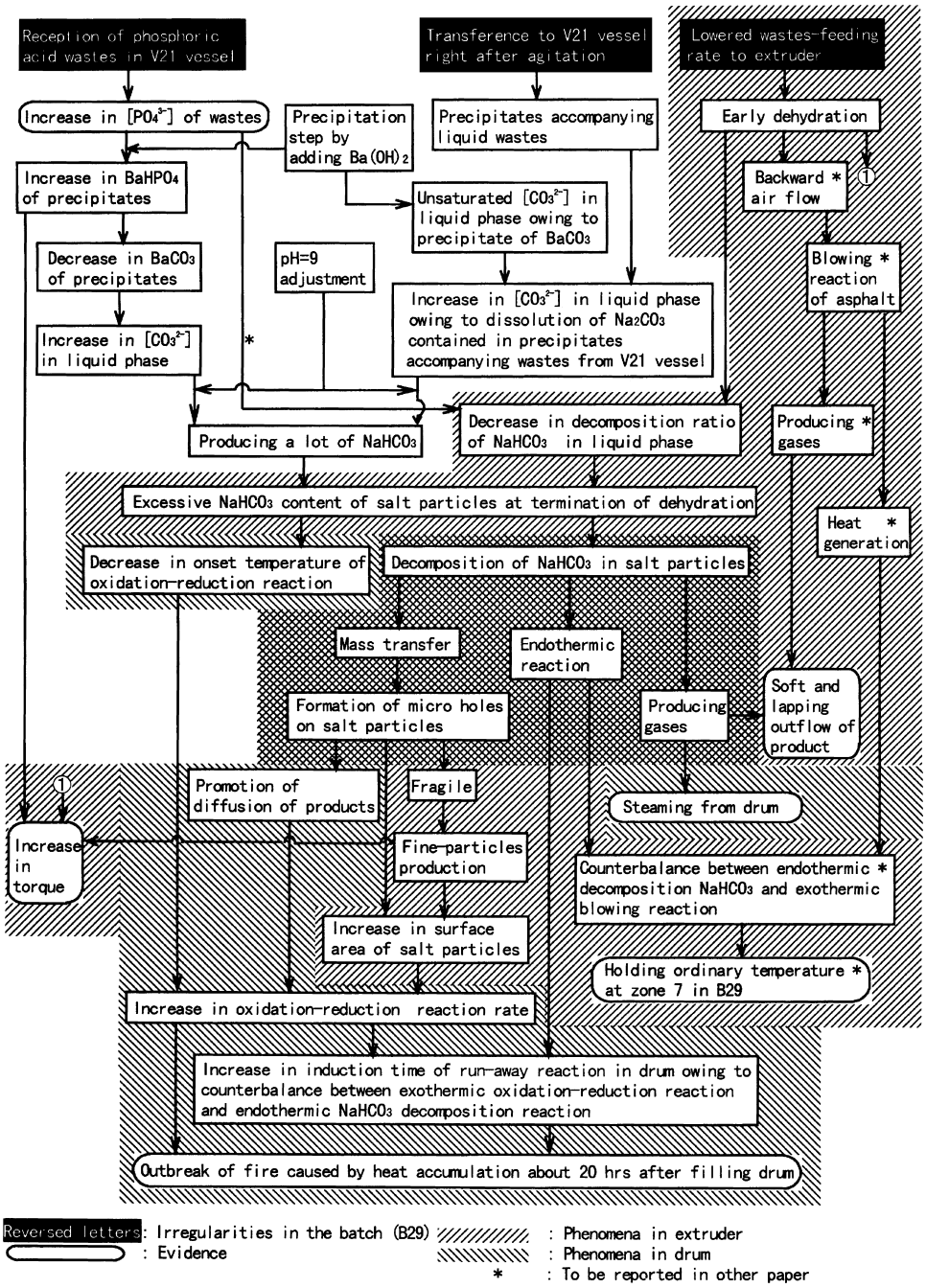

Fig. 14. Schematic of the causes of the outbreak of fire in BDF drums.

- Several hours after a drum was first filled, a dome-shaped surface of the waste product in the drum had been observed. The usual surface is flat or hollow.
- When the unburned drums from batch B29 were investigated in detail, an abnormal cavity or subsidence was found.

The above evidence is consistent with the postulated process leading to inclusion of a certain amount of sodium hydrogencarbonate in the salt particles at the end of the dehydration step and decomposition of this sodium hydrogencarbonate.

6. Conclusions and causality

The mechanism of ignition of bituminized low level radioactive waste, resulting in a fire and explosion at the BDF in the PNC Tokai Works, Japan, on 11 March, 1997 was clarified. In conclusion, the mechanism is outlined as follows.

1. In regard to an oxidation–reduction reaction of dried salt waste and asphalt, sodium nitrite plays the principal role of oxidant. The reaction, which is an interfacial reaction, determines the MTRR of a drum filled with the bituminized waste product.
2. Non-oxidizing salt molecules containing intramolecular hydrogen chemically decrease the onset temperature of the exothermic reaction between sodium nitrite and asphalt. The presence of sodium hydrogencarbonate results in a physical phenomenon that causes the heat release rate to be remarkably high. This physical phenomenon is disruption of the salt particle structure by gases resulting from sodium hydrogencarbonate decomposition. The resultant porous salt particle structure facilitates a fast reactant diffusion rate that increases the rate of the exothermic reaction.
3. As a result, there is a possibility that the MTRR can be significantly lower than the drum filling temperature of about 180°C in spite of the usual calculated MTRR of approximately 208°C. The existence of sodium hydrogencarbonate in the salt particles when dehydration ends in the extruder is thus a major contributing factor to a low MTRR.
4. There were three irregularities with respect to the standard operating conditions for batch B29. Each of these contributes to a build up of sodium hydrogencarbonate in the salt particles.
5. Much of the observational evidence is consistent with the existence of sodium hydrogencarbonate in the salt particles.

Based on the above descriptions, the relationships between the determined causes and effects are summarized in Fig. 14.

List of symbols

A	frequency factor (s^{-1})
Area	interfacial area per oxidizing mole (m^2/mol)
C_p	specific heat (J/K/g)
D	diffusion constant (s^{-1})
d	interfacial thickness per oxidizing mole (cm)
dH/dt	over all heat flow (J/s)
E	activation energy (J/mol)
g	gravity acceleration (cm/s^2)

ΔH_R	heat of reaction per unit mass of initial reactant or per oxidizing mole (J/g)
h	heat transfer coefficient from Nu (J/cm^2/s/K)
k	reaction rate constant (s^{-1})
L	height of drum (cm)
M	mass or mole number of oxidizer of reactant (g)
Nu	Nusselt number
$O_{balance}$	oxygen balance
Pr	Prandtl number
$\dot{q}$	rate of heat generation per unit volume (J/ml/s)
R	gas constant (J/K/mol)
R_0	radius of drum (cm)
r	radius of spherical particle or radial axis of drum (cm)
S	salt or contact area of system (cm^2)
T	temperature (K)
t	time (s)
V	interfacial volume per oxidizing mole (ml/mol)
x	conversion ratio
Y	rearranged expression

Greek letters

α	temperature conductivity (cm^2/s)
β	$1/T$ (K^{-1})
γ	correlation coefficient
κ	thermal conductivity (J/cm/s/K)
ν	kinetic viscosity (cm^2/s)
ρ	density (g/ml)
δ	thickness of diffusion layer (cm)
[ ]	concentration (mol/ml)

Subscripts

a	contact area of system
D	diffusion
d	drum
EX	exthothermicity
HC	heat capacity
HE	heat exchange
i	initial
p	pseudo zero-order reaction
R	reaction
surface	interface
w	wall
0	initiation or surroundings
∞	surroundings

References

[1] An investigative committee for the fire and explosion in the Bituminization Demonstration Facility (BDF) of the reprocessing plant of the Tokai Works of the Power Reactor and Nuclear Fuel Development Corporation (PNC), A report on the fire and explosion in BDF of the reprocessing plant of the Tokai Works of PNC, Nuclear Safety Bureau, Science & Technology Agency of Japan, 15 December, 1997 (in Japanese).
[2] M. Demonie, E. Detilleux, H. Eschrich, W. Hild, A. Osipenco, R. Reynders, The Fire Incident in the Eurobitum Plant on December 15, 1991 — Description, Evaluation and Conclusions, 1990.
[3] Y. Li, K. Hasegawa, in: The Proceedings of 9th International Symposium on Loss Prevention and Safety Promotion in the Process Industries, Barcelona, Spain, 4–8 May 1998, Editorial Graficas Signo, S.A., Barcelona, 1998, pp. II-555–569.
[4] K. Hata (Ed.), Kagakubenran (Handbook of Chemistry), Maruzen, Tokyo, 1984, pp. II-333 (in Japanese).